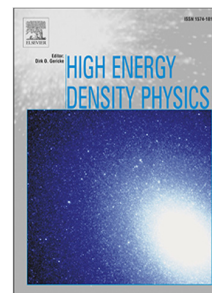


Journal Pre-proof

Mykonos: A pulsed power driver for science and innovation

Jens Schwarz, Brian Hutsel, Tom Awe, Bruno Bauer, Jacob Banasek, Eric Breden, Joe Chen, Michael Cuneo, Katherine Chandler, Karen De Zetter, Mark Gilmore, Matthew Gomez, Hannah Hasson, Maren Hatch, Nathan Hines, Trevor Hutchinson, Deanna Jaramillo, Christine Kalogeras Loney, Ian Kern, Derek Lamppa, Diego Lucero, Larry Lucero, Keith LeChien, Mike Mazarakis, Tommy Mulville, Robert Obregon, John Porter, Pablo Reyes, Daniel Scoglietti, Gabriel Shipley, Trevor Smith, Brian Stoltzfus, William Stygar, Adam Steiner, David Yager-Elorriaga, Kevin Yates



PII: S1574-1818(24)00069-7
DOI: <https://doi.org/10.1016/j.hedp.2024.101144>
Reference: HEDP 101144

To appear in: *High Energy Density Physics*

Please cite this article as: J. Schwarz, B. Hutsel, T. Awe et al., Mykonos: A pulsed power driver for science and innovation, *High Energy Density Physics* (2024), doi: <https://doi.org/10.1016/j.hedp.2024.101144>.

This is a PDF file of an article that has undergone enhancements after acceptance, such as the addition of a cover page and metadata, and formatting for readability, but it is not yet the definitive version of record. This version will undergo additional copyediting, typesetting and review before it is published in its final form, but we are providing this version to give early visibility of the article. Please note that, during the production process, errors may be discovered which could affect the content, and all legal disclaimers that apply to the journal pertain.

© 2024 Published by Elsevier B.V.

Mykonos: A pulsed power driver for science and innovation

Jens Schwarz^a, Brian Hutsel^a, Tom Awe^a, Bruno Bauer^f, Jacob Banasek^a, Eric Breden^a, Joe Chen^c, Michael Cuneo^a, Katherine Chandler^a, Karen De Zetter^a, Mark Gilmore^b, Matthew Gomez^a, Hannah Hasson^a, Maren Hatch^{a,b}, Nathan Hines^{a,b}, Trevor Hutchinson^d, Deanna Jaramillo^a, Christine Kalogeras Loney^{a,b}, Ian Kern^{a,b}, Derek Lamppa^a, Diego Lucero^a, Larry Lucero^a, Keith LeChien^e, Mike Mazarakis^a, Tommy Mulville^a, Robert Obregon^a, John Porter^a, Pablo Reyes^a, Daniel Scoglietti^a, Gabriel Shipley^a, Trevor Smith^{a,c}, Brian Stoltzfus^a, William Stygar^d, Adam Steiner^a, David Yager-Elorriaga^a and Kevin Yates^a

^aSandia National Laboratories, P.O. Box 5800, MS 1195, Albuquerque, 87185, NM, USA

^bThe University of New Mexico, Electrical and Computer Engineering Department, Albuquerque, 87131, NM, USA

^cUniversity of Michigan, Plasmas, Pulsed Power, and Microwave Laboratory, Ann Arbor, 48109, MI, USA

^dLawrence Livermore National Laboratory, , Livermore, 94550, CA, USA

^ePacific Fusion, , Fremont, 94538, CA, USA

^fUniversity of Nevada, Physics Department, Reno, 89557, NV, USA

ARTICLE INFO

Keywords:

Pulsed Power

ZNetUS

Linear Transformer Driver

ABSTRACT

Sandia National Laboratories has been operating the Mykonos linear transformer driver (LTD) in a five-cavity configuration since 2014. The machine operates at 1 MA output current, 500 kV output voltage, with a 10-90 % current rise time of 85 ns, which enables small scale physics and engineering pulsed power experiments. Mykonos provides hands-on pulsed power experimental training for students and staff along-side senior Sandia scientists in an environment that is more accessible than the Z Facility. Over the years, we have fielded and accumulated a wide variety of optical, x-ray and electrical diagnostics and we are preparing to open this facility to outside users.

Here, we are presenting the pulsed power and diagnostic capability of Mykonos as well as some recent experiments that have been performed on the facility. The goal of this publication is to attract researchers across the pulsed power and high energy density (HED) community to collaborate with Sandia on exciting, innovative science and to train the next generation of researchers for the National Nuclear Security Agency (NNSA) and the nation. As such, we have established a Mykonos Academic Access Program (MAAP) as part of ZNetUS to enable academic utilization of the Mykonos Pulsed Power Facility.

1. Mykonos Pulsed Power Driver

The Mykonos Facility [1, 2, 3, 4, 5] is located in Tech Area IV at Sandia National Laboratories. The high bay has a square footage of 4054 ft² and houses the pulsed power driver and an EMI shielded control room (Fig. 1).


The Mykonos pulsed power driver consists of 5, three-meter-diameter LTD cavities. Each cavity contains 36 LTD bricks comprised of a 200 kV multi-gap switch and two 40 nF capacitors per brick. The five cavities are triggered sequentially and drive a matched impedance coaxial water transmission line. The cavities are triggered with a 6.6 ns delay between cavities to match the transit time of the power pulse in the water transmission line. The cavities and bricks are shown in Fig. 2. The LTD cavities are designed to operate at up to ± 100 kV charge voltage. At full charge voltage, Mykonos nominally produces a 1 MA, 500 kV pulse with a rise time (10%- 90%) of 85 ns and a pulse width (FWHM) of 160 ns into a 0.5 Ω matched load. In order to increase machine lifetime and reliability, we nominally operate the LTD driver at 80 kV charge voltage, resulting in 0.8 MA of peak current.

2. Experimental Work Area

The experimental work area has a rectangular square footage of 12 \times 8 ft² and is fully enclosed and certified as a laser control area (LCA). The target chamber is mounted to the vacuum insulator at a height of 6 ft (center line), and is surrounded by a 8 \times 7 ft² optical breadboard along the wall that allows for flexible diagnostics configurations (Fig. 3). Two, 2-level optical tables are located on each side of the target chamber wall, having an area of 3 \times 6 ft² and 2.5 \times 5 ft² respectively. An additional optical table (4 \times 8 ft²) is available just outside the LCA for target preparation and diagnostic staging.

3. Standard Diagnostics

The list below includes diagnostics that have been fielded at the Mykonos Facility. Most of them will be available at any given time, except for those that are shared with the Z Facility. Experimenters will need to work closely with their Sandia counterpart when requesting or bringing in diagnostics.

 jschwarz@sandia.gov (J. Schwarz)

ORCID(s):

Mykonos

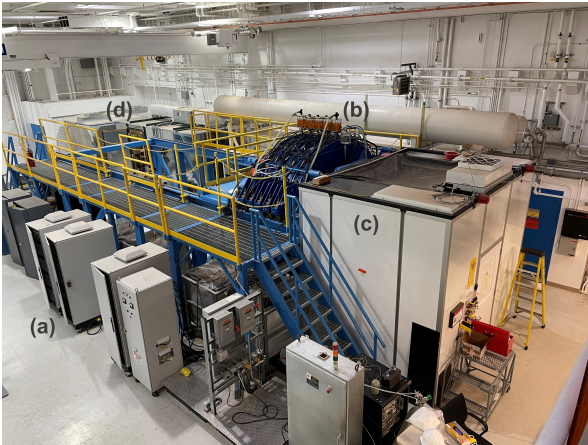


Figure 1: Bird's eye view of the Mykonos Facility. One can see the power supply racks for charging the capacitors in the front (a), with the five LTD cavities on the other side of the raised walkway (b). To the right is the laser controlled area (LCA) (c) that houses the target chamber (Fig. 3), lasers for diagnostics, optical breadboards, and various diagnostic instruments. The control room (d) is in the far back corner and blocked from view.

Optical Diagnostics:

- Four-frame pulsed laser imaging system (170 ps pulsed laser, 5-ns inter-pulse delay) at 1064 nm, 532 nm, 355 nm, and 266 nm.
 - Interferometry
 - Shadowgraphy
 - Schlieren
 - Angular Filter Refractometry
- Avalanche photodiode (APD) and other diode detectors (time-resolved self-emission, filterable)
- Two single-frame Andor iStar ICCDs; Minimum Exposure Time: 2-3 ns
- Four-frame ICCD camera
 - Specialized Imaging Model SIMX4
 - Exposure Time: 3 ns - 10 ms in 1 ns steps
 - Inter-frame Time: 0 ns - 20 ms in 1 ns steps
- Eight-frame ICCD
 - Cordin Model 222
 - Exposure Time: 2.5 ns - 10 ms
 - Inter-frame Time: 0 ns - 10 ms in 250 ps steps
- Twelve-frame Ultra High Speed Framing Camera (requires coordination with the ECE department of the University of New Mexico)
 - Invisible Vision UHSi 12/24
 - Exposure Time: 5 ns - 1 ms in 5 ns steps

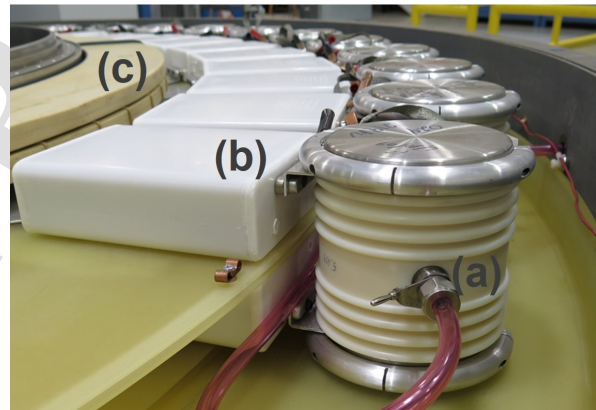
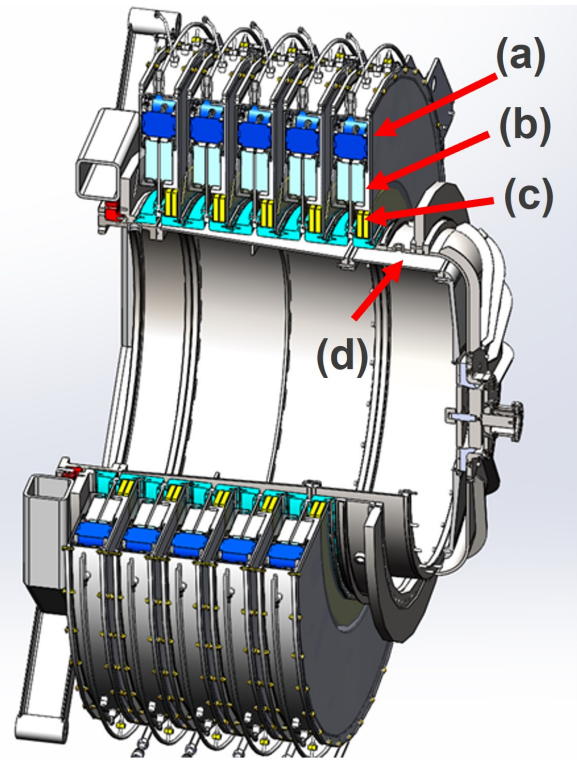


Figure 2: (top) Cross-section of a five cavity LTD, (bottom) Internal view of cavity showing LTD bricks. (a) 200 kV switch, (b) 40 nF capacitor pair, (c) iron core for inductive coupling into the (d) water-filled transmission line.

- Inter-frame Time: 0 ns - 10 ms in 5 ns steps
- Questar QM100 Long-Distance Microscope assemblies for imaging of $\approx 1\mu\text{m}$ phenomena
- Streaked Visible Spectroscopy (SVS)
- Two-color dispersion interferometer (in commissioning phase)
- Gated visible spectroscopy (1D spatial distribution)
- Gated Vacuum Ultraviolet (VUV) Spectroscopy (1D spatial distribution)

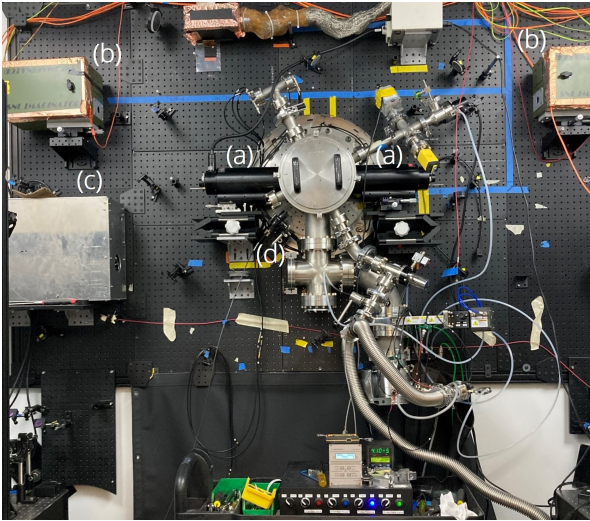


Figure 3: View of the Mykonos target chamber (center). Multiple lines of sight are available for various diagnostics. (a) Long-distance microscope, (b) single-frame ICCD, (c) 12-frame ICCD, (d) fiber-coupled Avalanche Photo Diode array (APD).

X-ray Diagnostics:

- Filtered PIN diodes
- Support for image plate
- Ultra-fast x-ray imager (UXI) [6], (in commissioning phase)

Electrical Diagnostics:

- Standard machine diagnostics (machine current and voltage into vacuum chamber)
- Standard load B-dots (current into load region)
- Inductive voltage monitor (voltage into load region)
- Micro-B-dots (small field sensors for localized current measurements)

4. Selected experimental campaigns

Examples of previous academic projects include the assessment of vacuum effects on power flow [7, 3, 8], exploration of the electrothermal instability [9, 10, 11, 12, 13], demonstration of auto-magnetizing liners [14, 15, 16], laser activated dopant spectroscopy [17, 18], electrode contaminant mitigation [19], new current and plasma measurement techniques [20], and inductively driven x-pinchs [21]. Several projects were incorporated into Ph.D. dissertation topics for graduate students, including those supported through the Stockpile Stewardship Academic Alliance (SSAA), the Stewardship Science Graduate Fellowship (SSGF), and the Department of Energy National Nuclear Security Administration Laboratory Residency Graduate Fellowship (DOE NNSA LRGF).

4.1. Auto-magnetized liners

Magnetized Liner Inertial Fusion (MagLIF [22, 23, 24]) is a magneto-inertial fusion concept that uses a pulsed axial current from the Z machine that generates an azimuthal magnetic field which implodes a metallic liner (cylindrical tube) radially inward to compress pre-magnetized laser-preheated fuel. The 100 ns implosion is slow compared to conventional inertial confinement concepts; thus, MagLIF uses a strong axial magnetic field, B_z , embedded in the fuel prior to compression to limit thermal conduction losses to the cold liner. Additionally, the axial magnetic field reduces the areal density requirements of the fuel for achieving self-heating by trapping charged fusion particle products. Fuel pre-magnetization is provided by an azimuthal current in Helmholtz-like magnetic field coils [25] positioned external to the liner and power flow hardware. These coils can currently generate close to 20 T, but are not expected to reach beyond 30 T in the coming years. However, fields above 30 T may provide improved magneto-thermal insulation of the preheated fuel. In the auto-magnetizing (AutoMag) liner concept [26], the azimuthal and axial current flows have been integrated into the MagLIF liner to automatically generate an internal magnetic field while driving a radial implosion of the liner (Fig. 4). Fielding AutoMag liners in MagLIF experiments would remove the need for external field coils, enabling improved x-ray diagnostic access and enhanced current coupling to the z-pinch target. Aluminum liners with

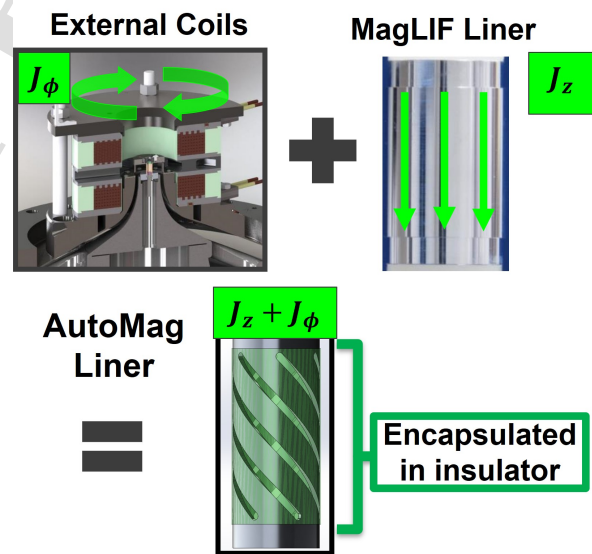


Figure 4: (top left) Present MagLIF hardware set, consisting of the final power feed leading up the the MagLIF liner at the center of the external field coils. The azimuthal current J_ϕ in the coils generates the axial magnetic field needed to trap the electrons, hence reducing thermal conduction losses; (top right) MagLIF liner (cylindrical tube) filled with deuterium fuel is radially compressed due to the axial current J_z provided by the Z accelerator. (bottom) AutoMag liner combines both current directions, creating an auto-generated internal magnetic field and a radial implosion.

various insulator-filled helical slot widths and pitch angles were fielded at the Mykonos driver. The charge voltage was varied from 50-90 kV, resulting in peak currents of 500-900 kA in a 100 ns pulse. In summary it was demonstrated that:

- An axial internal magnetic field greater than 90 T could be measured.
- The internal B-field strength depends on the pitch angle of the helical slots, i.e. shallow pitch angle leads to high B-field and vice versa.
- The timing of breakdown initiation is insensitive to varying the helical slot widths.

Once this concept was first proven out at the Mykonos pulsed power driver [14], it was then later fielded on the Z accelerator [15].

4.2. Development of X-Pinch radiography for Z

X-ray radiography is a diagnostic technique used to characterize the spatial distribution of mass within high energy density physics targets. On the Z facility, the Z-Beamlet laser [27] is used to generate the x-rays that image the magnetically driven target. This capability has enabled many physics studies [28, 29]. However, development of an additional x-ray radiography capability would provide several benefits. In experiments where the Z-Beamlet laser is used for another purpose (e.g., preheat in MagLIF [22]), it is not possible to also radiograph the implosion. An additional radiography source would also enable orthogonal imaging, which is useful for 3D stability studies.

On university-scale pulsed power systems, where kJ-class lasers are typically not available, X-pinchs are frequently used as the source for x-ray radiography [30, 31]. Establishment of an X-pinch-based radiography capability for the Z facility is underway [21] with much of the source development taking place on the Mykonos pulsed power facility. Mykonos is an ideal facility for this work because the current rise time (≈ 100 ns) and the peak current (≈ 900 kA) delivered to the target are a good match to the current available to drive an X-pinch on the Z facility [32].

An X-pinch produces x-rays from a small ($\approx 1 \mu\text{m}$) spot over a short (< 1 ns) duration. Emission is localized by only directing current to small radius for a short axial extent. X-pinchs take many forms; in this study we compare crossed wire, hybrid, and machined X-pinchs. Crossed wire X-pinchs are composed of two or more fine wires, which are twisted to form a single contact point (see Fig. 5a). In a hybrid X-pinch a single wire connects two conical electrodes (see Fig. 5c). A machined X-pinch consists of a single piece of material machined to create two cones connected by a small diameter “cross point” (see Fig. 5e). Details of the various load configurations are given in Table 1.

Crossed wires X-pinchs have been extensively studied, but the larger number of wires and smaller diameter wires add to the complexity, which makes fielding on the Z facility challenging. Hybrid X-pinchs are simpler to field but have a

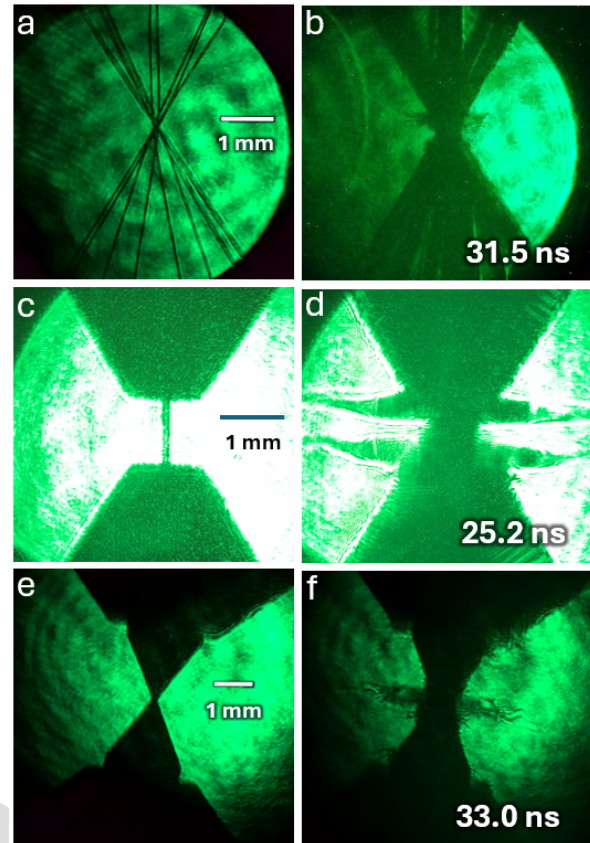


Figure 5: Laser shadowgraphs of crossed wire (a,b), hybrid (c,d), and machined (e,f) X-pinchs fielded on Mykonos. Pre-shot images are presented in (a), (c), and (e). Frame times for (d), (e), and (f) are given in the lower right corner. Spatial scales are provided for the hybrid and machined configurations are based on target features; the diagnostic aperture was used to set the crossed wire image magnification.

poor current contact between the wire and the cones, which may lead to more erratic performance than in crossed wire X-pinchs. Machined X-pinchs are more challenging to fabricate, but they eliminate challenges associated with the other X-pinch configurations. Experiments were conducted on the Mykonos facility to evaluate the performance of these different X-pinch configurations. Laser shadowgraphy was used to monitor the early-time plasma formation (Fig. 5), and x-ray diodes were used to monitor the x-ray emission history from the target (Fig. 6).

From the x-ray diode traces it is clear that the machined X-pinch did not perform as intended. Both the crossed wire and hybrid X-pinch configurations generated an initial x-ray spike around 55 ns, consistent with expectations based on Π -parameter scaling from previous X-pinch studies [33]. The machined X-pinch did not generate any measurable x-rays during the current pulse.

Laser shadowgraphy shows that with the crossed wire configuration plasma disks form above and below the crossing point, and a narrower region forms between them. In previous studies [34], it was shown that this smaller region

Table 1

Details for the three X-pinch configurations used to collect the shadowgraphy in Fig. 5 and x-ray emission histories in Fig. 6 are given. Wire material, number of wires, wire diameter, and mass per length at the crossing point/narrowest region [m/L] is listed for these three experiments. * Wire diameter listed for the machined X-pinch is the minimum diameter at the cross point.

	Crossed Wire	Hybrid	Machined
Shot #	13429	14833	11026
Material	Mo	Mo	Ti
# wires	8	1	N/A
wire dia. [μm]	35	102	105*
m/L [mg/cm]	0.79	0.83	0.39

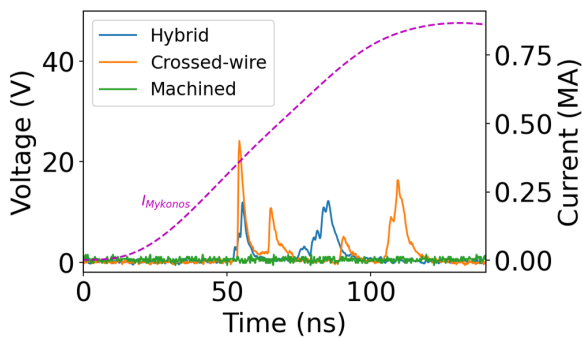


Figure 6: X-ray diode traces for the hybrid, crossed wire, and machined X-pinch configurations described in Table 1. A representative current trace for these experiments is also provided (dotted line).

forms a micro-pinch and generates x-rays. In the hybrid configuration, again there are two plasma disks which form at approximately the contact points between the cones and wire, and there is a narrower region between these plasma disks, which is expected to be the location of the micro-pinch. For the machined X-pinch, a plasma disk appears to form where the target was initially narrowest. A narrower region does not form, likely preventing the formation of a micro-pinch and ultimately stopping any significant x-ray emission.

Crossed wire experiments were also conducted with $4 \times 70 \mu\text{m}$ diameter Ti wires (0.69 mg/cm). These experiments produced x-rays at the expected time, ruling out X-pinch material as the source of poor performance for the machined X-pinches. Additionally, a machined X-pinch experiment conducted with a $160 \mu\text{m}$ diameter cross point (0.91 mg/cm) did not produce x-rays, ruling out the difference in m/L. The remaining hypothesis is that the machined X-pinch geometry is the source of poor performance. Based on these studies, development of both crossed wire and hybrid X-pinch configurations for use on the Z facility are underway.

4.3. Electrothermal Instability Research

The Electrothermal Instability (ETI) is an ohmic heating-driven instability, caused by the dependence of electrical

resistivity on temperature [35, 36, 37, 38]. Any inhomogeneity which alters current density, including surface defects or variations in local resistivity, can provide a seed for ETI growth. It can lead to non-uniform and premature plasma formation on conductor surfaces that can limit shot target performance and lead to decreasing transmitted energy, which may degrade applications such as Inertial Confinement Fusion (ICF), high pressure dynamic material properties experiments, and radiation effects science platforms [39]. ETI is known to provide a seed for Magneto-Rayleigh-Taylor (MRT) instabilities. Hence, understanding this instability is vital to its mitigation and to the improvement of HED applications.

We developed an ETI platform on Mykonos for the study of ohmically heated aluminum [10]. The ultra-pure (99.999%) aluminum barbell with a baseline surface roughness of less than 15 nm was heated over 100 ns by an electrical peak current of 900 kA (Fig. 7). Engineered defects (i.e. divots) of varying diameter, depth, spacing, and relative orientation were investigated, both for bare metal and below dielectric coatings [11]. Separate experiments with sinusoidal machined grooves of wavelength λ , and amplitude A , were also performed. Self-emission images are captured at a time resolution of 3 ns and a spatial resolution of $3 \mu\text{m}$. It was shown that micro-meter scale divots do indeed seed

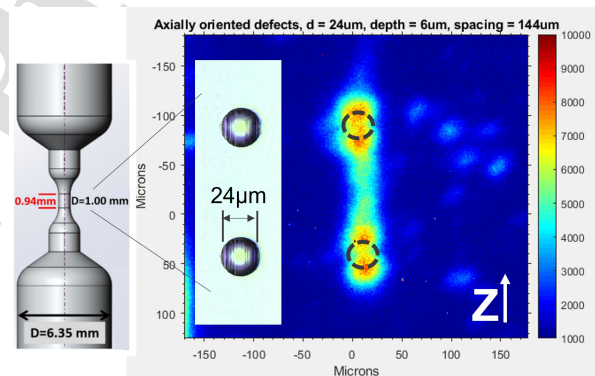


Figure 7: (left) Ultra-pure aluminum barbell with various engineered defects, (right) example of divot pair and associated thermal self-emission. One can see the so called “cat-eye” feature above and below the defects where the brightness increases due to current bunching up. Later in the current pulse, the defects merge to form axial striations and filaments.

local overheating and that their relative orientation dictates global plasma evolution. Sinusoidal surface perturbations show more intense surface heating for large A/λ ratios, in agreement with theory. Ongoing experiments have added a helical return can to the ETI platform to add an axial field component at the z physics target’s surface. Data is intended to provide new information about the helical instability observed in axially-premagnetized liner implosions [40, 41]. These experiments set the stage for “ride-along” experiments that were fielded on the Z machine this year.

4.4. Demonstration of in-situ plasma cleaning

In situ plasma cleaning is one promising approach for mitigating current loss in the inner magnetically insulated transmission line (MITL) of Sandia's Z machine. The idea is that an 80% argon and 20% oxygen mix would be driven by an audio square wave at background pressures of 0.1-1 Torr. This gas mix would then release lightly bound contaminants into the power flow gap where they would subsequently react with the oxygen to be pumped out. A prototype system, suitable for operation on Z, has been commissioned on the Mykonos Facility. [19]. We used the well established "Mykonos Parallel Plate Platform (MP3)" (Fig. 8). It is

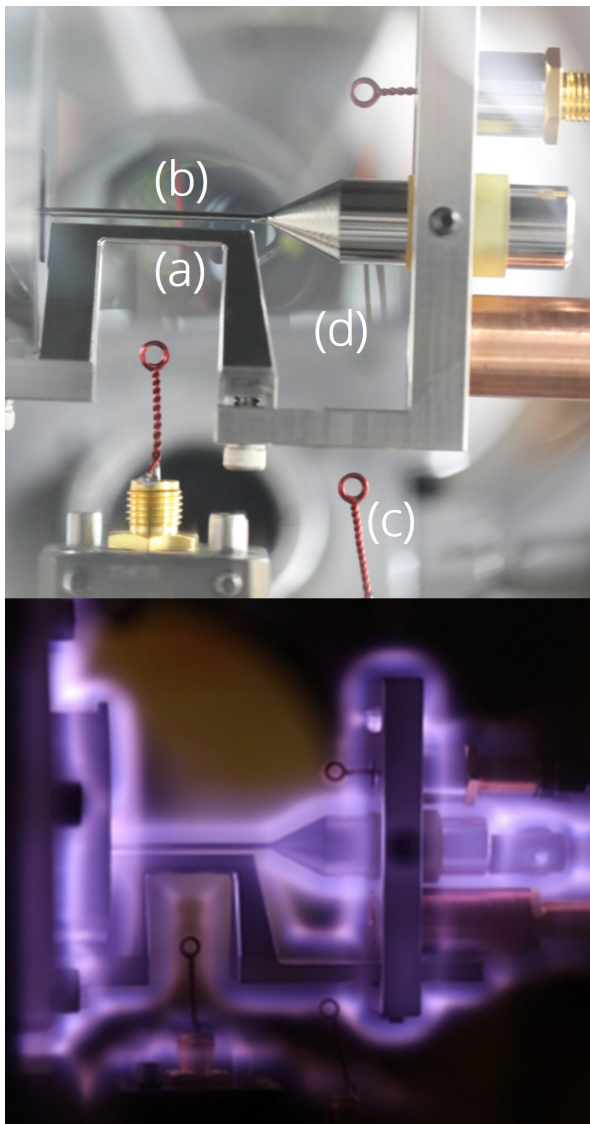


Figure 8: (top) Picture of the MP3 with the anode (a), cathode (b) pair, various B-dot probes (c), and the inductive load region (d); (bottom) Plasma glow discharge of an argon, oxygen mix during in-situ discharge cleaning.

designed to simultaneously achieve lineal current densities comparable to Z and provide multiple lines of sight to the power flow gap and electrode surfaces. The hardware

transitions from the axisymmetric geometry of Mykonos down to rod-like electrodes with elliptical (cathode) and trapezoidal (anode) cross sections. The cathode geometry was chosen to improve current density uniformity in the anode-cathode (AK) gap. The anode's profile was chosen for structural integrity and ease of machining. When assembled, they form a narrow AK gap (0.5-2 mm), high-field-stress transmission line that accesses MITL conditions of interest to higher energy accelerators. A downstream inductive load region is used to increase electric field stresses in the MITL.

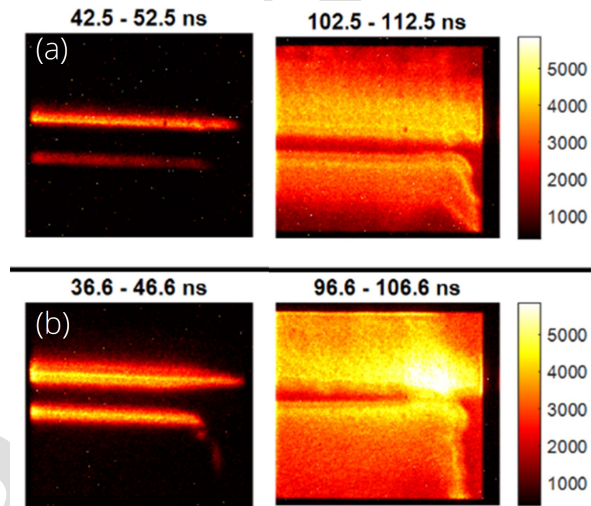


Figure 9: ICCD images of plasma formation near 50% and near 100% of peak current for a 0.5 mm AK gap that had been cleaned (a) and left untreated (b).

Figure 9 shows the benefits of plasma cleaning for a 0.5 mm AK gap that has been cleaned (a) versus left untreated (b). It can be seen that plasma formation on the untreated ("dirty") AK gap surface occurs sooner and is much brighter at 50% of peak current compared to the "clean" hardware. This becomes even more pronounced around peak current when the untreated hardware exhibits plasma breakdown while the "clean" hardware did still efficiently conduct current. Based on our APD measurements (not shown here), it appears that the onset of plasma emission and gap closure is delayed by at least 15 ns, which is important as it allows current delivery up to peak current with minimal losses. This cleaning approach will be fielded on Z, once it has been fully proven and optimized on MP3.

4.5. Development of low density plasma diagnostics

Our standard parallel plate platform (see section 4.4) was used to develop a fiber-based dispersion interferometer [20] that is designed to enable the first direct measurements of electrode plasma on the Z accelerator in the coming years. This detection scheme (Fig. 10) is first fielded on the Mykonos Facility and relies on the measurement of

the relative phase shift of two colinear, two color beams traversing the plasma of interest (estimated between 10^{14} – 10^{18} e⁻/cm²).

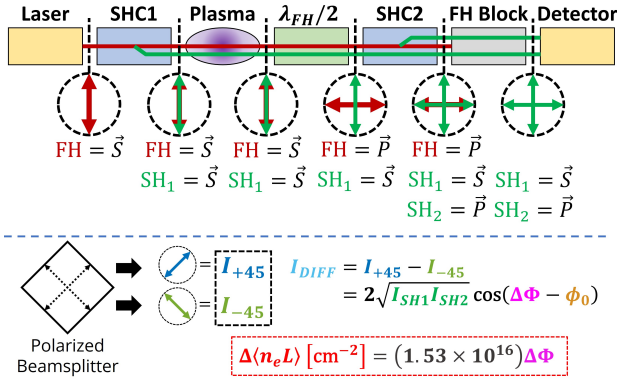


Figure 10: Schematic of a dispersion interferometer.

The First-Harmonic (FH), s-polarized, 1550 nm continuous wave (CW) beam is frequency doubled to 775 nm at the first Second-Harmonic Crystal (SHC1) and sent through a plasma, together with the unconverted collinear fundamental wavelength. Each beam experiences a different phase-shift that is measured downstream after frequency doubling the remaining fundamental wavelength at SHC2. After exiting a half-waveplate, the two orthogonally polarized SH waves are then passed through a polarizing beamsplitter rotated by 45° to split equal components of the SH waves. This splitting generates two waves with respective intensities I_{+45} & I_{-45} , whose difference is directly related to the difference in phase shift $\Delta\Phi$ between the first and second-harmonic beam. For expected electron densities far below the critical plasma density (4.6×10^{20} cm⁻³), the phase shift $\Delta\Phi$ is proportional to the electron line density. Presently, the lower bound of electron areal density sensitivity is limited to 8.5×10^{14} cm⁻². Future work on Mykonos is planned to bolster sensitivity by increasing the signal to noise ratio.

For initial experiments, the probe beam was focused down to between 50-350 μm diameter and placed just below the cathode at the location above the anode knee (i.e. the plasma breakdown location in Fig. 9(b) right). Figure 11 shows data gathered during a small temporal window that covers the plasma turn-on time to the point where the signal is lost due to significant plasma absorption and refraction. One can see that the plasma goes from undetected to about 1.5×10^{16} e⁻/cm² in less than 5 ns at 75 ns into the pulse when the accelerator exceeds 400 kA. From there, the density briefly drops to 1×10^{16} e⁻/cm² over the following 10 ns at which point it rises again sharply to over 3×10^{16} e⁻/cm². The rapid fluctuation in electron density is most likely due to the rapidly evolving, non-uniform plasma that is being probed at that location (Fig. 11). Furthermore, the plasma experiences an $E \times B$ drift velocity that drives the surface plasma toward the load region, causing local fluctuations in plasma density.

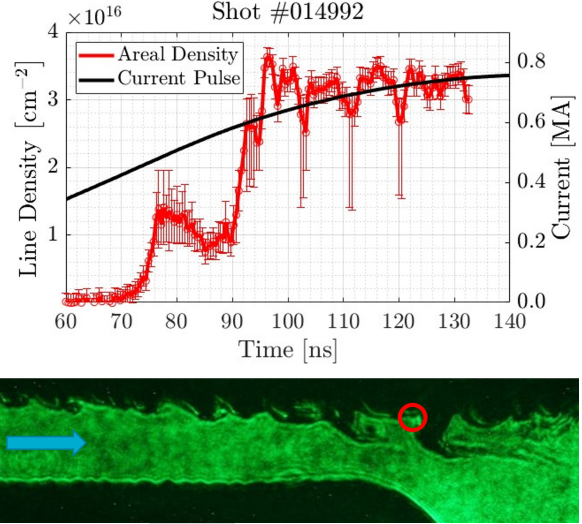


Figure 11: (top) Measured electron line density (red) and drive current (black) as a function of time; (bottom) Laser shadowgraphy image of top cathode and lower anode knee around the time of peak current. The red circle depicts the location of the probe beam and the blue arrow shows the direction of the $E \times B$ flow.

5. Future Outlook: MAAP and ZNetUS

Pulsed power science and technology is an important research area that supports several NNSA missions including HED plasma physics, radiation effects science, and inertial confinement fusion. A recent tri-laboratory report as well as recent external advisory and review boards recommended a significant expansion of partnerships with universities to meet critical recruiting pipelines in this field over the next decade. In response to this report, the ZNetUS consortium [42] was established to encourage collaboration between research scientists in academia, national laboratories, and industry that support long-term growth in pulsed power science and related HED physics research.

As such, we have created the Mykonos Academic Access Program (MAAP) as part of ZNetUS to enable academic utilization of the Mykonos Pulsed Power Facility. We seek to expand the partnerships between students and research scientists in academia and the national laboratories. This will enhance recruiting in pulsed power and HED science to support long-term growth in pulsed power science and related HED physics research. We see the MAAP as a partnership between Sandia and the academic collaborators with the goal to field excellent experiments and advance novel diagnostic capabilities.

6. Summary

We have presented a brief overview of the Mykonos facility at Sandia National Laboratories. With several shots per day, large breadth of diagnostics, and 1 MA (500 kV) drive current to a matched load, it is an attractive medium-scale

pulsed power driver that allows students to be “hands-on” while they perform world-class research under the guidance of experienced staff members. Our organization cares deeply about the development of future talent in pulsed power and HED science and has hence established the MAAP. We are looking forward to welcoming academic institutions around the country in pursuit of scientific excellence.

7. Acknowledgments

We would like to recognize the tremendous work over the past ten years that has transformed the Mykonos facility from a technology demonstrator into the vibrant research facility that it is today. Many researchers and students, supported by LDRD, NNSA stipends, and program funding have steadily improved infrastructure and diagnostics to a world-class level.

This work was supported by the Laboratory Directed Research and Development program at Sandia National Laboratories, a multimission laboratory managed and operated by National Technology and Engineering Solutions of Sandia LLC, a wholly owned subsidiary of Honeywell International Inc. for the U.S. Department of Energy’s National Nuclear Security Administration under contract DE-NA0003525. This paper describes objective technical results and analysis. Any subjective views or opinions that might be expressed in the paper do not necessarily represent the views of the U.S. Department of Energy or the United States Government.

References

- [1] M. G. Mazarakis, W. E. Fowler, A. A. Kim, V. A. Sinebryukhov, S. T. Rogowski, R. A. Sharpe, D. H. McDaniel, C. L. Olson, J. L. Porter, K. W. Struve, W. A. Stygar, J. R. Woodworth, High current, 0.5-MA, fast, 100-ns, linear transformer driver experiments, *Physical Review Special Topics-Accelerators and Beams* 12 (2009) 050401.
- [2] M. G. Mazarakis, W. E. Fowler, K. L. LeChien, F. W. Long, M. K. Matzen, D. H. McDaniel, R. G. McKee, C. L. Olson, J. L. Porter, S. T. Rogowski, K. W. Struve, W. A. Stygar, J. R. Woodworth, A. A. Kim, V. A. Sinebryukhov, R. M. Gilgenbach, M. R. Gomez, D. M. French, Y. Y. Lau, J. C. Zier, D. M. VanDevalde, R. A. Sharpe, K. Ward, High-current linear transformer driver development at sandia national laboratories, *IEEE Transactions on Plasma Science* 38 (2010) 704.
- [3] B. T. Hutsel, B. S. Stoltzfus, E. W. Breden, W. E. Fowler, P. A. Jones, D. W. Justus, F. W. Long, D. J. Lucero, K. A. MacRunnels, M. G. Mazarakis, J. L. Mckenney, J. K. Moore, T. D. Mulville, J. L. Porter, M. E. Savage, W. A. Stygar, Millimeter-gap magnetically insulated transmission line power flow experiments, in: 2015 IEEE Pulsed Power Conference (PPC), 2015, pp. 1–5. doi:10.1109/PPC.2015.7296902.
- [4] R. D. McBride, W. A. Stygar, M. E. Cuneo, D. B. Sinars, M. G. Mazarakis, J. J. Leckbee, M. E. Savage, B. T. Hutsel, J. D. Douglass, M. L. Kiefer, B. V. Oliver, G. R. Laity, M. R. Gomez, D. A. Yager-Elorriaga, S. G. Patel, B. M. Kovalchuk, A. A. Kim, P. A. Gourdain, S. N. Bland, S. Portillo, S. C. Bott-Suzuki, F. N. Beg, Y. Maron, R. B. Spielman, D. V. Rose, D. R. Welch, J. C. Zier, J. W. Schumer, J. B. Greenly, A. M. Covington, A. M. Steiner, P. C. Campbell, S. M. Miller, J. M. Woolstrum, N. B. Ramey, A. P. Shah, B. J. Sporer, N. M. Jordan, Y. Y. Lau, R. M. Gilgenbach, A primer on pulsed power and linear transformer drivers for high energy density physics applications, *IEEE Transactions on Plasma Science* 46 (2018) 3928–3967.
- [5] K. LeChien, M. Mazarakis, W. Fowler, W. Stygar, F. Long, R. McKee, G. Natoni, J. Porter, K. Androlewicz, T. Chavez, G. Feltz, V. Garcia, D. Guthrie, R. Mock, T. Montoya, J. Puissant, A. Smith, P. Wakeland, K. Ward, D. Van De Valde, A. Kim, A 1-mv, 1-ma, 0.1-hz linear transformer driver utilizing an internal water transmission line, in: 2009 IEEE Pulsed Power Conference, 2009, pp. 1186–1191. doi:10.1109/PPC.2009.5386430.
- [6] Q. Looker, A. P. Colombo, J. L. Porter, Detector thickness effects on nanosecond-gated imager response, *Review of Scientific Instruments* 92 (2021) 053504.
- [7] K. Tummel, A. J. Link, D. R. Welch, D. V. Rose, W. A. Stygar, B. T. Hutsel, K. R. LeChien, Power flow in magnetically insulated transmission lines with ion backscatter effects, *Physics of Plasmas* 30 (2023) 093506.
- [8] B. T. Hutsel, J. N. Gansz, D. M. Jaramillo, D. J. Lucero, J. Moore, D. V. Rose, W. A. Stygar, Current Loss in 0.1 - 100 Terawatt Vacuum Transmission Lines: Experiments and Simulations, Technical Report, 2018.
- [9] K. C. Yates, T. J. Awe, B. S. Bauer, T. M. Hutchinson, E. P. Yu, S. Fuelling, D. C. Lamppa, M. R. Weis, Initial surface conditions affecting the formation of plasma on metal conductors driven by a mega-ampere current pulse, *Physics of Plasmas* 27 (2020) 082707.
- [10] T. J. Awe, E. P. Yu, M. W. Hatch, T. M. Hutchinson, K. Tomlinson, W. D. Tatum, K. C. Yates, B. T. Hutsel, B. S. Bauer, Seeding the explosion of a high-current-density conductor in a controlled manner through the addition of micron-scale surface defects, *Physics of Plasmas* 28 (2021) 072104.
- [11] M. W. Hatch, T. J. Awe, E. P. Yu, T. M. Hutchinson, K. Yates, W. Tatum, K. Tomlinson, D. Yager-Elorriaga, B. T. Hutsel, B. S. Bauer, M. Gilmore, Fundamental studies on the electrothermal instability on the 1 MA mykonos driver*, 2020.
- [12] T. M. Hutchinson, T. J. Awe, B. S. Bauer, B. T. Hutsel, D. A. Yager-Elorriaga, K. C. Yates, A. W. Klemmer, M. W. Hatch, S. E. Kreher, E. P. Yu, M. Gilmore, On the relative importance of the different initial conditions that seed the electrothermal instability, *Journal of Applied Physics* 130 (2021) 153302.
- [13] E. P. Yu, T. J. Awe, K. R. Cochrane, K. C. Yates, T. M. Hutchinson, K. J. Peterson, B. S. Bauer, Use of hydrodynamic theory to estimate electrical current redistribution in metals, *Physics of Plasmas* 27 (2020) 052703.
- [14] G. A. Shipley, T. J. Awe, B. T. Hutsel, S. A. Slutz, D. C. Lamppa, J. B. Greenly, T. M. Hutchinson, Megagauss-level magnetic field production in cm-scale auto-magnetizing helical liners pulsed to 500 kA in 125 ns, *Physics of Plasmas* 25 (2018) 052703.
- [15] G. A. Shipley, T. J. Awe, B. T. Hutsel, J. B. Greenly, C. A. Jennings, S. A. Slutz, Implosion of auto-magnetizing helical liners on the Z facility, *Physics of Plasmas* 26 (2019) 052705.
- [16] G. A. Shipley, T. J. Awe, Three-dimensional magnetohydrodynamic modeling of auto-magnetizing liner implosions on the Z accelerator, *Physics of Plasmas* 30 (2023) 102707.
- [17] S. Patel, S. Simpson, Active Dopant Optical Spectroscopy via Laser Ablation for High Resolution Spectral Measurements, Technical Report, 2019.
- [18] S. Patel, B. T. Hutsel, A. M. Steiner, L. Perea, D. M. Jaramillo, Diagnosing Field Strengths and Plasma Conditions in Magnetically Insulated Transmission Lines Using Active Dopant Spectroscopy, Technical Report, 2020.
- [19] D. C. Lamppa, S. C. Simpson, B. T. Hutsel, G. R. Laity, M. E. Cuneo, D. V. Rose, Assessment of Electrode Contamination Mitigation at 0.5 MA Scale, Technical Report, 2021.
- [20] N. R. Hines, S. Patel, D. Scoglietti, M. Gilmore, S. L. Billingsley, R. H. Dwyer, T. Awe, D. Armstrong, D. Bliss, G. Laity, M. Cuneo, A fiber-coupled dispersion interferometer for density measurements of pulsed power transmission line electron sheaths on sandia’s z machine, *Rev. Sci. Instrum.* 93 (2022) 113505.

- [21] C. E. Myers, M. R. Gomez, D. C. Lamppa, T. J. Webb, D. A. Yager-Elorriaga, B. T. Hutsel, C. A. Jennings, P. Knapp, M. R. Kossow, L. M. Lucero, R. J. Obregon, A. M. Steiner, First demonstration of an inductively driven X-pinch for diagnosing high energy density experiments on the Z pulsed power facility, 2020.
- [22] S. A. Slutz, M. C. Herrmann, R. A. Vesey, A. B. Sefkow, D. B. Sinars, D. C. Rovang, K. J. Peterson, M. E. Cuneo, Pulsed-power-driven cylindrical liner implosions of laser preheated fuel magnetized with an axial field, *Physics of Plasmas* 17 (2010) 056303.
- [23] M. R. Gomez, S. A. Slutz, A. B. Sefkow, K. D. Hahn, S. B. Hansen, P. F. Knapp, P. F. Schmit, C. L. Ruiz, D. B. Sinars, E. C. Harding, C. A. Jennings, T. J. Awe, M. Geissel, D. C. Rovang, I. C. Smith, G. A. Chandler, G. W. Cooper, M. E. Cuneo, A. J. Harvey-Thompson, M. C. Herrmann, M. H. Hess, D. C. Lamppa, M. R. Martin, R. D. McBride, K. J. Peterson, J. L. Porter, G. A. Rochau, M. E. Savage, D. G. Schroen, W. A. Stygar, R. A. Vesey, Demonstration of thermonuclear conditions in magnetized liner inertial fusion experiments, *Physics of Plasmas* (1994-present) 22 (2015) 056306.
- [24] D. A. Yager-Elorriaga, M. R. Gomez, D. E. Ruiz, S. A. Slutz, A. J. Harvey-Thompson, C. A. Jennings, P. F. Knapp, P. F. Schmit, M. R. Weis, T. J. Awe, G. A. Chandler, M. Mangan, C. E. Myers, J. R. Fein, B. R. Galloway, M. Geissel, M. E. Glinsky, S. B. Hansen, E. C. Harding, D. C. Lamppa, W. E. Lewis, P. K. Rambo, G. K. Robertson, M. E. Savage, G. A. Shipley, I. C. Smith, J. Schwarz, D. J. Ampleford, K. Beckwith, K. J. Peterson, J. L. Porter, G. A. Rochau, D. B. Sinars, An overview of magneto-inertial fusion on the Z machine at sandia national laboratories, *Nuclear Fusion* 62 (2022) 042015.
- [25] D. C. Rovang, D. C. Lamppa, M. E. Cuneo, A. C. Owen, J. McKenney, D. W. Johnson, S. Radovich, R. J. Kaye, R. D. McBride, C. S. Alexander, T. J. Awe, S. A. Slutz, A. B. Sefkow, T. A. Haill, P. A. Jones, J. W. Argo, D. G. Dalton, G. K. Robertson, E. M. Waisman, D. B. Sinars, J. Meissner, M. Milhous, D. N. Nguyen, C. H. Mielke, Pulsed-coil magnet systems for applying uniform 10–30 t fields to centimeter-scale targets on sandia's z facility, *Review of Scientific Instruments* 85 (2014) 124701.
- [26] S. A. Slutz, C. A. Jennings, T. J. Awe, G. A. Shipley, B. T. Hutsel, D. C. Lamppa, Auto-magnetizing liners for magnetized inertial fusion, *Physics of Plasmas* 24 (2017) 012704.
- [27] P. Rambo, I. Smith, J. Porter, M. Hurst, C. Speas, R. Adams, A. Garcia, E. Dawson, B. Thurston, C. Wakefield, J. Kellogg, M. Slattery, H. Ives, R. Broyles, J. Caird, A. Erlandson, J. Murray, W. Behrendt, N. Neilsen, J. Narduzzi, Z-Beamlet: A multikilojoule, terawatt-class laser system, *Applied Optics* 44 (2005) 2421–2430.
- [28] R. D. McBride, S. A. Slutz, C. A. Jennings, D. B. Sinars, M. E. Cuneo, M. C. Herrmann, R. W. Lemke, M. R. Martin, R. A. Vesey, K. J. Peterson, A. B. Sefkow, C. Nakhleh, B. E. Blue, K. Killebrew, D. Schroen, T. J. Rogers, A. Laspe, M. R. Lopez, I. C. Smith, B. W. Atherton, M. Savage, W. A. Stygar, J. L. Porter, Penetrating radiography of imploding and stagnating beryllium liners on the z accelerator, *Physical Review Letters* 109 (2012) 135004.
- [29] D. E. Ruiz, D. A. Yager-Elorriaga, K. J. Peterson, D. B. Sinars, M. R. Weis, D. G. Schroen, K. Tomlinson, J. R. Fein, K. Beckwith, Harmonic generation and inverse cascade in the z-pinch driven, preseeded multimode, magneto-rayleigh-taylor instability, *Phys. Rev. Lett.* 128 (2022) 255001.
- [30] J. D. Douglass, D. A. Hammer, Cobra-star, a five frame point-projection x-ray imaging system for IMA scale wire-array Z pinches, *Rev. Sci. Instrum.* 79 (2008) 033503.
- [31] J. Strucka, J. W. D. Halliday, T. Gheorghiu, H. Horton, B. Krawczyk, P. Moloney, S. Parker, G. Rowland, N. Schwartz, S. Stanislaus, S. Theocharous, C. Wilson, Z. Zhao, T. A. Shelkovenko, S. A. Pikuz, S. N. Bland, A portable X-pinch design for x-ray diagnostics of warm dense matter, *Matter and Radiation at Extremes* 7 (2021) 016901.
- [32] M. Gomez, C. Myers, M. Hatch, B. Hutsel, C. Jennings, D. Lamppa, M. Lowinske, A. Maurer, A. Steiner, K. Tomlinson, Developing an extended convolute post to drive an X-pinch for radiography at the Z facility, Technical Report, Sandia National Lab.(SNL-NM), Albuquerque, NM (United States), 2021.
- [33] D. D. Ryutov, M. S. Derzon, M. K. Matzen, The physics of fast z pinches, *Reviews of Modern Physics* 72 (2000) 167–223.
- [34] T. A. Shelkovenko, S. A. Pikuz, I. N. Tilikin, M. D. Mitchell, S. N. Bland, D. A. Hammer, Evolution of x-pinch loads for pulsed power generators with current from 50 to 5000 kA, *Matter and Radiation at Extremes* 3 (2018) 267–277.
- [35] T. M. Hutchinson, T. J. Awe, B. S. Bauer, D. H. Dolan, J. R. Pillars, B. T. Hutsel, E. P. Yu, A. W. Klemmer, S. E. Kreher, Photonic doppler velocimetry of ohmically exploded aluminum surfaces, *Physics of Plasmas* 27 (2020) 052705.
- [36] M. J. Carrier, W. A. Farmer, A. W. Klemmer, S. E. Kreher, B. S. Bauer, B. Srinivasan, Effect of surface roughness on phase transition timing in megaampere pulsed-power-driven exploding conductors, *Physics of Plasmas* 30 (2023) 092108.
- [37] E. Yu, T. Awe, K. Cochrane, K. Peterson, K. Yates, T. Hutchinson, M. Hatch, B. Bauer, K. Tomlinson, D. Sinars, Three-dimensional feedback processes in current-driven metal, *Physical Review E* 107 (2023) 065209.
- [38] E. Yu, T. Awe, K. Cochrane, K. Peterson, K. Yates, T. Hutchinson, M. Hatch, B. Bauer, K. Tomlinson, D. Sinars, Seeding the electrothermal instability through a three-dimensional, nonlinear perturbation, *Physical Review Letters* 130 (2023) 255101.
- [39] D. B. Sinars, M. A. Sweeney, C. S. Alexander, D. J. Ampleford, T. Ao, J. P. Apruzese, C. Aragon, D. J. Armstrong, K. N. Austin, T. J. Awe, A. D. Baczewski, J. E. Bailey, K. L. Baker, C. R. Ball, H. T. Barclay, S. Beatty, K. Beckwith, K. S. Bell, J. F. Benage Jr., N. L. Bennett, K. Blaha, D. E. Bliss, J. J. Boerner, C. J. Bourdon, B. A. Branch, J. L. Brown, E. M. Campbell, R. B. Campbell, D. G. Chacon, G. A. Chandler, K. Chandler, P. J. Christenson, M. D. Christison, E. B. Christner, R. C. Clay, K. R. Cochrane, A. P. Colombo, B. M. Cook, C. A. Coverdale, M. E. Cuneo, J. S. Custer, A. Dasgupta, J.-P. Davis, M. P. Desjarlais, D. H. Dolan, J. D. Douglass, G. S. Dunham, S. Duwal, A. D. Edens, M. J. Edwards, E. G. Evstatiev, B. G. Farfan, J. R. Fein, E. S. Field, J. A. Fisher, T. M. Flanagan, D. G. Flicker, M. D. Furnish, B. R. Galloway, P. D. Gard, T. A. Gardiner, M. Geissel, J. L. Giuliani, M. E. Glinsky, M. R. Gomez, T. Gomez, G. P. Grim, K. D. Hahn, T. A. Haill, N. D. Hamlin, J. H. Hammer, S. B. Hansen, H. L. Hanshaw, E. C. Harding, A. J. Harvey-Thompson, D. Headley, M. C. Herrmann, M. H. Hess, C. Highstrete, O. A. Hurricane, B. T. Hutsel, C. A. Jennings, O. M. Johns, D. Johnson, M. D. Johnston, B. M. Jones, M. C. Jones, P. A. Jones, P. E. Kalita, R. J. Kamm, J. W. Kellogg, M. L. Kiefer, M. W. Kimmel, P. F. Knapp, M. D. Knudson, A. Kreft, G. R. Laity, P. W. Lake, D. C. Lamppa, W. L. Langston, et al., Review of pulsed power-driven high energy density physics research on z at sandia, *Physics of Plasmas* 27 (2020) 070501.
- [40] T. J. Awe, R. D. McBride, C. A. Jennings, D. C. Lamppa, M. R. Martin, D. C. Rovang, S. A. Slutz, M. E. Cuneo, A. C. Owen, D. B. Sinars, K. Tomlinson, M. R. Gomez, S. B. Hansen, M. C. Herrmann, J. L. McKenney, C. Nakhleh, G. K. Robertson, G. A. Rochau, M. E. Savage, D. G. Schroen, W. A. Stygar, Observations of modified three-dimensional instability structure for imploding z-pinch liners that are pre-magnetized with an axial field, *Physical Review Letters* 111 (2013) 235005.
- [41] T. J. Awe, C. A. Jennings, R. D. McBride, M. E. Cuneo, D. C. Lamppa, M. R. Martin, D. C. Rovang, D. B. Sinars, S. A. Slutz, A. C. Owen, K. Tomlinson, M. R. Gomez, S. B. Hansen, M. C. Herrmann, M. C. Jones, J. L. McKenney, G. K. Robertson, G. A. Rochau, M. E. Savage, D. G. Schroen, W. A. Stygar, Modified helix-like instability structure on imploding Z-pinch liners that are pre-imposed with a uniform axial magnetic field, *Physics of Plasmas* 21 (2014) 056303.
- [42] ZNetUS, 2022. <https://znetus.eng.ucsd.edu>.

Declaration of interests

The authors declare that they have no known competing financial interests or personal relationships that could have appeared to influence the work reported in this paper.

The authors declare the following financial interests/personal relationships which may be considered as potential competing interests:

Journal Pre-proof